Vectorial perturbation theory for axisymmetric whispering gallery resonators

B. Sturman,[1] E. Podivilov,[1,2] C. S. Werner,[3] and I. Breunig[3,4,*]

[1]*Institute of Automation and Electrometry, Russian Academy of Sciences, 630090 Novosibirsk, Russia*

[2]*Novosibirsk State University, Novosibirsk 630090, Russia*

[3]*University of Freiburg, IMTEK, Georges-Köhler-Allee 102, 79110 Freiburg, Germany*

[4]*Fraunhofer Institute for Physical Measurement Techniques IPM, Heidenhofstraße 8, 79110 Freiburg, Germany*

(Received 11 October 2018; published 3 January 2019)

We propose a vectorial perturbation theory for axially symmetric, generally nonspherical whispering gallery resonators made of isotropic and anisotropic optical materials. It is based on analysis of the leading terms in the coupled equations for independent light-field components, as derived from Maxwell's equations, and true boundary conditions. Strong localization of the whispering gallery modes (WGMs) near the resonator rim, controlled by the azimuth modal number m, is the main prerequisite for our analysis. The theory gives high-precision expressions for the WGM frequencies and modal functions, including the evanescent effects. One of important applications of the theory is analysis of anticrossings of the WGM resonances in anisotropic resonators detected in experiments. Simple relations for the frequency avoidance gaps during the anticrossings are derived and compared with experimental data obtained in lithium-niobate-based WGM resonators. We show also that the vectorial effects substantially restrict the field of applicability of the scalar WGM models.

DOI: 10.1103/PhysRevA.99.013810

I. INTRODUCTION

Optical microresonators currently attract strong research interest because of numerous important effects and applications, ranging from sensing of single atoms and molecules to quantum and nonlinear optics [1–16]. They all are due to the presence of whispering gallery modes (WGMs) propagating along the resonator rim and possessing very high Q factors (up to 10^{11}) and very small mode volumes. Correspondingly, the WGM frequency spectrum is quasidiscrete, and a strong intensity enhancement inside the resonator occurs owing to the resonant recirculation. The methods for coupling light in and out of the resonators are well developed [2,3,16].

Except for special cases [17,18], the resonators are axisymmetric and characterized by the major radius R. Their shape and size, as well as optical properties of the matrix, vary strongly [1,2,5,14–16]. In the simplest case, the shape is spherical and the matrix is isotropic. Angle-cut WGM resonators made of isotropic materials are known as well [14]; their sizes are some tens of micrometers. For a broad category of millimeter-sized crystalline resonators fabricated by turning, the shape is nonspherical [5–7,16]. Near the rim it can be characterized by the major radius R and the minor radius r. Furthermore, millimeter-sized resonators are often designed for nonlinear $\chi^{(2)}$ applications, such as second harmonic generation and optical parametric oscillation, and made of uniaxial crystals. In this case, the optical axis coincides with the rotational one.

Vectorial WGM solutions to Maxwell's equations, i.e., solutions for the electric ($\boldsymbol{E}$) and magnetic ($\boldsymbol{H}$) light fields, are available only for spherical resonators made of isotropic materials [3,16,19–21]. Here, the vectorial problem is reduced to a solution of the scalar Helmholtz equation, and the modes can be treated as transverse-electric (TE) and transverse-magnetic (TM) ones. The existing approaches to the description of WGMs in anisotropic resonators are impractically complicated, even for the spherical geometry [22–24]. The only general simplification for $\boldsymbol{E}$ and $\boldsymbol{H}$ in the axisymmetric case is a separation of the phase factor $\exp(im\varphi - i\omega t)$, where φ is the azimuth angle, m is the azimuth number, and ω is the angular WGM frequency.

Regardless of specific features of axisymmetric resonators, the optical WGMs can be viewed as quasi plane waves propagating along the resonator rim with the wave vector m/R and localized thus in the equatorial plane. This means that the polar modal numbers are modest [20] and the scale of spatial changes along the rim (R/m) is much shorter than the transverse localization scales inside the resonator. Also, this means that the azimuth number can be approximately expressed by the vacuum wavelength λ: $m \simeq 2\pi Rn/\lambda$, where n is the refractive index. For $R = 1$ mm, $n = 2$, and $\lambda = 1\ \mu$m we have $m \approx 10^4$. Such huge values of the azimuth number m enable one to develop perturbation analysis.

While solid theoretical grounds for analysis of WGMs in nonspherical and anisotropic resonators are absent, high-Q modes are still there. Scalar models, ignoring the vectorial effects, are widely accepted for analysis of WGMs [25–28]. As in the spherical case, each mode is characterized here not only by the azimuth number m, but also by the radial and polar numbers q and p, so that $\omega = \omega(m, q, p)$. The scalar models involve complicated treatments of the scalar Helmholtz and eikonal equations in curvilinear coordinates—spheroidal, toroidal, etc. [29,30]. Their main outcomes are expressions for ω as a power series in $m^{-1/3}$ up to the terms of the order of m^{-1}. This corresponds to the calculation accuracy $\delta\omega/\omega \approx$

*Corresponding author: ingo.breunig@imtek.de

m^{-2}. In anisotropic resonators, the scalar models are applied to the ordinary (o) and extraordinary (e) WGMs characterized by the refractive indices n_o and n_e. This implies that the field $\boldsymbol{E}$ is almost perpendicular and parallel to the optical axis. The model predictions have allowed experimentalists to identify WGMs in isotropic and anisotropic resonators [18,31,32].

Importantly, the above scalar models and expressions for WGM frequencies have no direct connection with Maxwell's equations and the air-resonator boundary conditions (BCs) for $\boldsymbol{E}$ and $\boldsymbol{H}$. In essence, they are semiphenomenological. In particular, the scalar Helmholtz equation used to be solved with zero Dirichlet BCs at the resonator rim [25,26]. After that, corrections to the WGM frequencies are postulated to account phenomenologically for the evanescent fields outside the resonator. The scalar approach based on the eikonal equation [27] has the same semiphenomenological status. Numerical tools for vectorial solutions are in progress [33,34]; however, they are still insufficient for full-scale analysis of WGMs with $m \gtrsim 10^4$.

Often useful, the scalar models fail completely to describe anticrossings of the o and e modes in anisotropic resonators. This general effect is of strong practical interest because of its relevance to the mode control and tuning capabilities of WGM resonators. Imagine that we change the temperature T. Then different dependences $n_o(T)$ and $n_e(T)$ lead to crossings of the primary o and e resonances, i.e., to the equality $\omega_o(m_o, q_o, p_o) = \omega_e(m_e, q_e, p_e)$ for numerous combinations of the modal numbers. Similar crossings occur for other tuning techniques [16]. Near the crossing points, the o and e modes can strongly interact with each other (vectorial coupling) by analogy with the quantum-mechanical crossing [35] and with crossings of classical resonances [36]. Generally, two scenarios are possible—crossing and anticrossing (avoided crossing). Which of them comes true depends on the symmetry properties of the modes [35]. In the WGM case, the situation simplifies: Because of the axial symmetry, the modes with different azimuth numbers, $m_o \neq m_e$, are independent and cannot interact with each other. Thus, the anticrossings are allowed only for $m_o = m_e$. The anticrossings of WGMs occur regularly in experiments with anisotropic resonators [16,37,38]. They are usually attributed to remnant cross-polarization scattering, regardless of the vectorial coupling.

Analysis of the anticrossing behavior requires a systematic approach to the vectorial WGM effects. Development of such an approach is our main methodical goal. In particular, this approach must clarify the validity of the scalar models. Let us stress that vectorial WGM coupling is present already in the case of isotropic optical material. The point is that the spatial derivatives in orthogonal curvilinear coordinate systems act not only on the field components, but also on the basis vectors, leading to a mutual coupling of the field components. An important simplifying circumstance is strong localization of WGMs near the resonator rim. It allows us to keep the leading scalar and vectorial terms and see the calculation accuracy in a fairly simple manner.

The frequency avoidance gaps during the anticrossings should not be mixed up with the splits of WGM frequencies caused by perturbations breaking the axial symmetry [16,39].

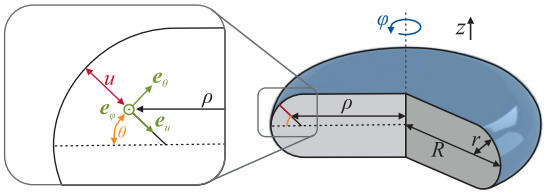

FIG. 1. Geometry of a WGM resonator: R and r are the major and minor radii, u and θ are the local cross-sectional coordinates, φ is the azimuth angle, $\rho = \rho(u, \theta)$ is the distance to the symmetry axis, and $\boldsymbol{e}_u$, $\boldsymbol{e}_\theta$, $\boldsymbol{e}_\varphi$ are the unit basis vectors.

The latter have nothing to do with the frequency tuning and vectorial effects. Another interesting but entirely different system possessing the anticrossing behavior is photonic structures representing chains of resonantly coupled microspheres [40,41].

II. ESSENTIALS OF SCALAR MODELS

Here we present essentials of the scalar models for an axisymmetric nonspherical resonator characterized by the major and minor curvature radii R and r, see Fig. 1, and made of an isotropic material. The radii ratio $\eta = R/r$ is expected to be of the order of 1. Our procedure is a substantially advanced version of that presented in [28], and it is strongly different from the approach of [25–27]. It allows one to see the main spatial scales relevant to WGMs and the main idea of the subsequent vectorial perturbation analysis.

Let the scalar WGM amplitude $A = A(\boldsymbol{r})$ obey the Helmholtz equation

$$(\Delta + n^2 k^2)A = 0, \tag{1}$$

where Δ is the Laplacian, n is the refractive index, $k = \omega/c$, and c is the speed of light. The physical nature of A is unimportant at this stage. By solving Eq. (1) with certain BCs, we have to find the allowed values of ω (or k^2) and the corresponding modal distributions $A(\boldsymbol{r})$.

Below we employ the orthogonal curvilinear coordinate system u, θ, φ depicted in Fig. 1. Here u is the distance to the boundary, θ is the polar angle measured from the equator, and $\rho = \rho(u, \theta)$ is the distance to the symmetry axis. The corresponding scaling (Lame) coefficients are $h_u = 1$, $h_\theta = r - u$, and $h_\varphi = \rho$. They are φ independent owing to the axial symmetry. As soon as $u \ll r$ and $\theta \ll 1$ within the range of WGM localization, the distance ρ can be expanded in a series in u and θ. Further details are considered below.

Using the general expression for Δ in orthogonal curvilinear coordinates [42] and splitting off the factor $\exp(im\varphi)$, we have the following for $A = A(u, \theta)$:

$$\left[\frac{1}{\rho h_\theta}\left(\frac{\partial}{\partial u}h_\theta \rho \frac{\partial}{\partial u} + \frac{\partial}{\partial \theta}\frac{\rho}{h_\theta}\frac{\partial}{\partial \theta}\right) - \frac{m^2}{\rho^2} + n^2 k^2\right]A = 0. \tag{2}$$

Let u_m and θ_m be the characteristic localization scales of $A(u, \theta)$ in u and θ. They are expected to be much smaller than r and 1, respectively. The scale of changes along the rim, R/m, must be the smallest. We expect thus that $\eta/m \ll u_m/r \ll 1$ and $\eta/m \ll \theta_m \ll 1$. If so, the last two terms in

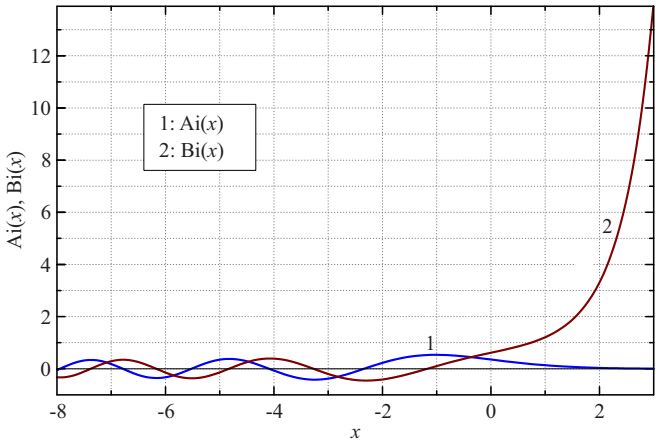

FIG. 2. Behavior of the Airy functions $\mathrm{Ai}(x)$ and $\mathrm{Bi}(x)$ for modest values of the argument x.

Eq. (2) are the largest and they strongly compensate each other. In the leading WGM approximation, it is necessary therefore (i) to keep the first terms in the expansion of $1/\rho^2$ in u and θ and (ii) to keep only the leading contribution in each of the differential terms. The higher-order terms will be treated then as small perturbations. In the differential terms, we neglect the derivatives of h_θ and $h_\varphi = \rho$ in favor of derivatives of the rapidly changing amplitude $A(u,\theta)$. This results in the replacement of the Laplacian Δ in Eqs. (1) and (2) by

$$\Delta_0 = \frac{\partial^2}{\partial u^2} + \frac{1}{r^2}\frac{\partial^2}{\partial \theta^2} - \frac{m^2}{R^2}\left(1 + \frac{2u}{R} + \frac{r\theta^2}{R}\right). \qquad (3)$$

Employing the variable separation, we obtain [20,28] that $A = \Theta_p(\theta/\theta_m)U(u/u_m)$, where $p = 0, 1, \ldots$ is the polar number, $\Theta_p(x)$ is the pth wave function of the quantum oscillator [35], such that $\int \Theta_p^2(x)\,dx = 1$, while

$$u_m = R/(2m^2)^{1/3} \quad \text{and} \quad \theta_m = \eta^{3/4}/m^{1/2} \qquad (4)$$

are the localization scales inside the resonator. The differential equation for the radial function $U(u/u_m)$ is reduced to the Airy equation $y'' = xy$. The latter admits two fundamental solutions [43,44], $\mathrm{Ai}(x)$ and $\mathrm{Bi}(x)$, rapidly decreasing and increasing with x, see Fig. 2.

Only the Ai function provides a rapid decrease of U with increasing u. Correspondingly, we have $U = C\mathrm{Ai}(a + u/u_m)$, where C is a constant,

$$a = (m/2)^{2/3}[1 + (2p+1)\sqrt{\eta}/m - X], \qquad (5)$$

and $X = (n\omega R/cm)^2$ is a convenient dimensionless frequency parameter. As follows from Eqs. (4), the expected inequalities for u_m and θ_m are well fulfilled for $m \gtrsim 10^3$.

By following [25,26], we employ now the Dirichlet BC $U(0) = 0$. Then we have $a = -\zeta_q$, where ζ_q is the qth zero of $\mathrm{Ai}(-\zeta)$: $\zeta_q \simeq 2.338,\ 4.088, \ldots$, and $X = X_0$, where

$$X_0 = 1 + (2/m)^{2/3}\,\zeta_q + \sqrt{\eta}\,(2p+1)/m. \qquad (6)$$

Thus, we have found the zero-order frequency parameter and modal functions. The constant C can be chosen arbitrary for any radial number q, so that we have a set of radial functions

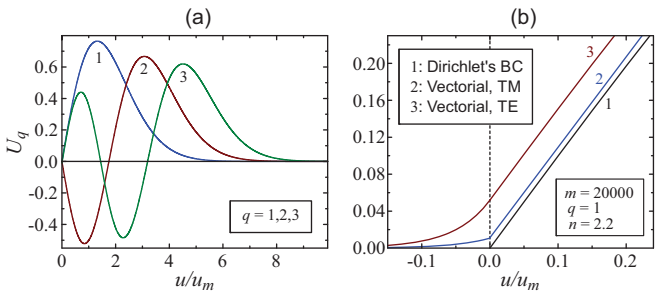

FIG. 3. (a) First three normalized radial functions $U_q(u/u_m)$ for Dirichlet's BC, and (b) modification of the function $U_1(u/u_m)$ near the rim owing to air-dielectric BCs for $m = 2\times10^4$ and $n = 2.2$. Lines 2 and 3 correspond to the TM and TE modes.

$U_q(u/u_m) = C_q\mathrm{Ai}(u/u_m - \zeta_q)$. It is convenient to choose C_q such that $\int_0^\infty U_q^2(y)\,dy = 1$. The radial functions meet the orthogonality relation $\int_0^\infty U_{q_1}(y)U_{q_2}(y)dy = \delta_{q_1,q_2}$ and $C_q = 1/|\mathrm{Ai}'(-\zeta_q)|$, see Appendix A.

The first three radial functions are illustrated in Fig. 3(a). For $R \approx 1$ mm and $m \approx 10^4$, they are localized near the rim on a micrometer scale.

Not only Dirichlet's but also Neumann's BC $U'(0) = 0$ can be employed. The latter can be attributed to the perfect-conductor environment. To change to the Neumann BC in the above relations for X_0 and U_q, it is sufficient to replace ζ_q by zeros ζ_q' of the derivative of $\mathrm{Ai}'(-\zeta)$. The corresponding radial functions are also strongly localized near the rim and meet the orthogonality relation, see Appendix A.

None of Dirichlet's and Neumann's BCs correspond to true air-resonator BCs. Moreover, there is no way to employ the air-resonator BCs within the scalar approach for nonspherical geometries. One might try to employ the Helmholtz equation (1) outside the resonator, where $u < 0$, by changing $n \to 1$. Here we must use the second fundamental solution of the Airy equation, $\mathrm{Bi}(x)$ [43,44], to provide a rapid decrease of the scalar amplitude $A(u)$ with increasing $|u|$. However, any single BC at $u = 0$ is insufficient to describe $A(u)$ for $u \lessgtr 0$ and determine ω. Analysis of the evanescent effects becomes possible only in the vectorial case; see the next section. Nevertheless, analysis of the scalar case with Dirichlet's and Neumann's BCs is important for what follows.

Now we switch to perturbation analysis. To do so, we set $\Delta = \Delta_0 + \Delta_1$ in Eq. (1). The perturbation Δ_1 accounts for corrections to Δ_0 within Eq. (2). Using the estimates $\partial A/\partial u \sim A/u_m$ and $\partial A/\partial\theta \sim A/\theta_m$, we see from Eqs. (3) and (4) that Δ_0 includes terms up to the order of m. Our aim is to increase calculation accuracy up to terms larger than m^0. We account for higher-order terms in the expansion of $\rho^{-2}(u,\theta)$ and for the spatial derivatives of the Lame coefficients $h_\varphi = \rho$ and h_θ. One can check that the necessary accuracy is achieved with

$$\Delta_1 = \frac{m^2}{R^2}\left[\frac{3u^2}{R^2} + \frac{u\theta^2}{R}\left(\frac{3}{\eta} - 1\right)\right] - \frac{2\eta^3 u}{R^3}\frac{\partial^2}{\partial\theta^2}. \qquad (7)$$

The differential term comes from an expansion of $h_\theta^{-2}(u)$. The first contribution to Δ_1 can be estimated as $\sim m^{2/3}$, while the second and third terms are $\sim m^{1/3}$. Other contributions to Δ

are $\sim m^0$ or smaller. Equation (7) is fairly general: It can be used for any resonator shape that can be characterized by the major and minor curvature radii R and r. In particular, it is applicable to the toroidal and spheroidal shapes. The shape features that cannot by described by R and r correspond to the higher-order corrections to Δ. Generally, the expansion of $\rho^{-2}(\theta, u)$ includes a term proportional θ^3; it is nonzero in the absence of top-bottom symmetry. This θ^3 term gives, however, zero-frequency correction within the first-order perturbation theory. This is why it is omitted.

Setting now the frequency parameter $X = (n\omega R/cm)^2$ in the form $X = X_0 + X_1$, we can find the correction X_1 within the standard first-order perturbation theory [35] from Eq. (1): $X_1 = R^2\langle q, p|\Delta_1|q, p\rangle/m^2$. We have adopted the quantum-mechanical bra-ket notation, implying integration with $\Theta_p(x)U_q(y)$ over $x = \theta/\theta_m$ and $y = u/u_m$. Direct calculations show that

$$X_1 = \frac{2\zeta_q^2}{5}\left(\frac{2}{m}\right)^{4/3} + \frac{(2p+1)\zeta_q\sqrt{\eta}(\eta+3)}{12}\left(\frac{2}{m}\right)^{5/3} \quad (8)$$

for Dirichlet's BC. These calculations employ certain identities for integrals of the Airy functions (see Appendix A). The second-order corrections to X are negligible within the necessary calculation accuracy.

Finally, we find an expression for ω that accounts for the terms of the order up to $m^{-2/3}$. Using the relation $\sqrt{1+x} \simeq 1 + x/2 - x^2/8$, we obtain in the Dirichlet case

$$\frac{\omega Rn}{c} = m + \zeta_q\left(\frac{m}{2}\right)^{1/3} + \frac{(2p+1)\sqrt{\eta}}{2} + \frac{3\zeta_q^2}{20}\left(\frac{2}{m}\right)^{1/3} + \frac{(2p+1)\eta^{3/2}\zeta_q}{12}\left(\frac{2}{m}\right)^{2/3}. \quad (9)$$

All terms of this dispersion relation coincide with the corresponding terms of Eq. (19) of [27]. Furthermore, one can check that the case of a sphere $\eta = 1$, where an expansion of ω^2 in m can be easily obtained, nicely corresponds to the known results. To switch to Neumann's BC, it is sufficient to change $\zeta_q \to \zeta_q'$ in Eqs. (8) and (9).

Thus, we have obtained all actual terms for ω within the standard first-order perturbation theory without employment of special models and mathematical methods. Most probably, analysis of smaller corrections to ω ($\delta\omega/\omega \lesssim 1/m^2$) within the scalar Helmholtz equation is useless. The point is that the vectorial effects give similar corrections to ω (see Sec. III).

Changing from the Dirichlet to true air-resonator BCs results in addition of certain evanescent correction terms in Eq. (9). They are derived in the next section.

III. VECTORIAL EFFECTS, ISOTROPIC CASE

A. Choice of independent variables

In the case of an isotropic medium, the electric field amplitude $\boldsymbol{E}$ obeys the vectorial Helmholtz equation $(\Delta + k^2n^2)\boldsymbol{E} = 0$ inside the resonator. Furthermore, it obeys the solenoidality condition $\nabla \cdot \boldsymbol{E} = 0$. The same general relations are valid for the magnetic field amplitude $\boldsymbol{H}$. In air, it is sufficient to change $n \to 1$.

In the general nonspherical case, any two field components can be chosen as independent variables, and the remaining components are expressible by this pair from Maxwell's equations. The choice of independent variables is greatly a matter of convenience.

One can start from the components $E_{u,\theta,\varphi}$ in our curvilinear u, θ, φ coordinate system. In this case $\boldsymbol{E} = \boldsymbol{e}_u E_u + \boldsymbol{e}_\theta E_\theta + \boldsymbol{e}_\varphi E_\varphi$, where $\boldsymbol{e}_u, \boldsymbol{e}_\theta, \boldsymbol{e}_\varphi$ are the unit basis vectors (see Fig. 1). Not only the field components, but also the basis vectors $\boldsymbol{e}_{u,\theta,\varphi}$ depend on the coordinates. The axial symmetry allows us again to split off the factor $\exp(im\varphi)$ for all components. However, the vector $\boldsymbol{E}$ *is not* proportional to $\exp(im\varphi)$. The Laplacian Δ in the Helmholtz equation acts both on the field components and basis vectors, leading to three coupled equations for $E_{u,\theta,\varphi}$. The component E_φ can be expressed by $E_{u,\theta}$ from the solenoidality condition. Thus, we can obtain two coupled φ-independent partial differential equations for E_u and E_θ. They have to be solved with the known air-dielectric boundary conditions. These conditions also show coupling between E_u and E_θ. Thus, we have two different coupling sources—the bulk of the resonator and its boundary $u = 0$. The same situation occurs if we chose $H_{u,\theta}$ as independent variables.

Another choice, which is preferable for our studies, is employment of the field components E_z and H_z as independent variables. Each of these components obey the same scalar Helmholtz equation (1), so that the bulk coupling is absent, regardless of any approximations.

Generally, WGMs can be treated as quasi-TE and quasi-TM modes. For them, E_z and H_z are the largest among the electric and magnetic field components inside the resonator, and they can be taken as scalar modal amplitudes.

B. Boundary conditions for E_z and H_z

Our procedure of derivation of the BCs at $u = 0$ is perturbative. The coupling terms are derived in the leading approximation in powers of $1/m$, and the noncoupling terms have an accuracy sufficient to calculate the WGM frequencies (with the coupling neglected) up to terms larger than ω/m^2.

As known, vector $\boldsymbol{H}$ and the tangential components of $\boldsymbol{E}$ are continuous across the boundary. Thus, the set of independent initial BCs can be chosen as

$$H_{z1} = H_{z2}, \quad E_{\theta 1} = E_{\theta 2}, \quad E_{\varphi 1} = E_{\varphi 2}, \quad H_{\varphi 1} = H_{\varphi 2}, \quad (10)$$

where 1 and 2 refer to the dielectric and air sides of the boundary, respectively. Only the first BC is formulated for the z components, and it shows no coupling between H_z and E_z. Our task is to express the other BCs in terms of H_z and E_z.

To express $E_{\theta,\varphi}$ and H_φ by E_z and H_z, we need to know basic polarization properties of the TE and TM modes. They follow from Maxwell's equations. Inside the resonator we have $\nabla \times \boldsymbol{E} = ik\boldsymbol{H}$ and $\nabla \times \boldsymbol{H} = -ikn^2\boldsymbol{E}$; in air we must change $n \to 1$. Also, it is necessary to keep in mind that $nkR \simeq m$. For the TE modes we have $H_{u1} \simeq -nE_{\theta 1}$ in the dielectric and $H_{u2} \simeq -nE_{\theta 2}$, $H_{\varphi 2} \sim E_{\theta 2}$ in air; the other components are small in $1/m$. For the TM mode we have similarly $E_{u1} \simeq H_{\theta 1}/n$, $E_{u2} \simeq nH_{\theta 2}$, and $E_{\varphi 2} \sim H_{\theta 2}$ for the largest components. Large values of $E_{\varphi 2}$ and $H_{\varphi 2}$ are due to a rapid decrease of the evanescent fields in air. Now we can rewrite all BCs in terms of E_z and H_z.

First, we express E_θ by E_z and E_ρ: $E_\theta \simeq E_z - \theta E_\rho$, where E_ρ is the projection of $\boldsymbol{E}$ to the basis vector $\boldsymbol{e}_\rho$ of the cylindric ρ, φ, z coordinate system. This expression is geometrical; it is evident from Fig. 1 and valid both inside and outside the resonator. Analogously, we have $H_\theta \simeq H_z - \theta H_\rho$. Corrections to the coefficients of 1 before E_z and H_z would be $\sim\theta^2 \sim 1/m$; they give frequency corrections $\delta\omega \sim \omega/m^2$, (see also below).

Second, we indicate that $E_\rho \simeq -E_u$ and $H_\rho \simeq -H_u$ in the leading approximation in θ^2. This property is also geometrical (see Fig. 1). Thus, we have with a sufficient accuracy: $E_\theta \simeq E_z + \theta E_u$ and $H_\theta \simeq H_z + \theta H_u$. The coupling terms include a small parameter—the angle θ.

Third, we employ the above polarization properties of the TE and TM modes. Namely, we express E_u and H_u by H_z and E_z, respectively, in the coupling terms of the above expressions. After that we have

$$E_{\theta 1} \simeq E_{z1} + \theta H_{z1}/n, \quad E_{\theta 2} \simeq E_{z2} + n\theta H_{z2},$$
$$H_{\theta 1} \simeq H_{z1} - n\theta E_{z1}, \quad H_{\theta 2} \simeq H_{z2} - n\theta E_{z2}. \tag{11}$$

Fourth, we substitute these relations into Eqs. (10). Substitution into the BCs for the φ components requires some comments. Inside the resonator, we have from Maxwell's equations at $u = 0$:

$$H_{\varphi 1} \simeq -i(R\,\partial_u E_{\theta 1} - \eta\,\partial_\theta E_{u1})/kR,$$
$$E_{\varphi 1} \simeq i(R\,\partial_u H_{\theta 1} - \eta\,\partial_\theta H_{u1})/n^2 kR, \tag{12}$$

where $\partial_u = \partial/\partial u$ and $\partial_\theta = \partial/\partial\theta$. On the air side of the boundary, it is sufficient to change $1 \to 2$ and $n^2 \to 1$. According to Eqs. (12), the first terms in the expressions for H_φ and E_φ are the largest. In these large terms we must keep both contributions to E_θ and H_θ. In the smallest second terms, it is sufficient to substitute E_u and H_u in the leading approximation in θ. After all, we arrive at the final form of our BCs:

$$\begin{aligned} E_{z1} + \theta H_{z1}/n &= E_{z2} + n\theta H_{z2} \\ H_{z1} &= H_{z2} \\ \partial_u E_{z1} + \hat{K} H_{z1}/n &= \partial_u E_{z2} + n\hat{K} H_{z2} \\ \partial_u H_{z1} - n\hat{K} E_{z1} &= n^2 \partial_u H_{z2} - n^3 \hat{K} E_{z2}, \end{aligned} \tag{13}$$

where $\hat{K} = \theta\partial_u - (1/r)\partial_\theta$. The second terms in the right- and left-hand sides describe coupling between the TE and TM modes. The coupling terms in the first line are structurally different from those in lines 3 and 4.

C. WGM frequencies and modal functions

With the coupling terms neglected, we have independent BCs for the TE and TM modes: $E_{z1} = E_{z2}$, $\partial_u E_{z1} = \partial_u E_{z2}$ and $H_{z1} = H_{z2}$, $\partial_u H_{z1} = n^2 \partial_u H_{z2}$. We start from the TE case. As in Sec. II, we represent the Laplacian Δ as $\Delta_0 + \Delta_1$ and treat Δ_1 as a perturbation. The zero-order Helmholtz equation $(\Delta_0 + k^2 n^2)E_z = 0$ yields solutions for $E_{z1,z2}$ in the form

$$E_{z1} = c_1 \Theta_p \mathrm{Ai}(a_1 + u/u_m), \quad E_{z2} = c_2 \Theta_p \mathrm{Bi}(a_2 + u/u_m), \tag{14}$$

where $c_{1,2}$ are arbitrary constants, $\Theta_p(\theta/\theta_m)$ is the polar function, $\mathrm{Ai}(x)$ and $\mathrm{Bi}(x)$ are the fundamental solutions of the Airy equation (see Fig. 2), and

$$\begin{aligned} a_1 &= (m/2)^{2/3}[1 - X + \sqrt{\eta}\,(2p+1)/m] \\ a_2 &= (m/2)^{2/3}[1 - X/n^2 + \sqrt{\eta}\,(2p+1)/m]. \end{aligned} \tag{15}$$

Set (15) is just Eq. (5) applied to the dielectric and air parts. Substituting the expressions for E_{z1} and E_{z2} into the relevant BCs and taking the ratio, we easily get

$$\mathrm{Ai}(a_1)/\mathrm{Ai}'(a_1) = \mathrm{Bi}(a_2)/\mathrm{Bi}'(a_2). \tag{16}$$

This is a dispersion equation for $X = (kRn/m)^2$.

To analyze Eq. (16), we indicate that $X \simeq 1$ for the WGM solutions. According to Eqs. (15), this means that $a_2 \approx (m/2)^{2/3}(n^2-1)/n^2 \gg 1$. Using the asymptotic relation $\mathrm{Bi}(x) = (\pi^2 x)^{-1/4}\exp(2x^{3/2}/3)$ [43], which is well fulfilled for $x \gtrsim 2$, we obtain that $\mathrm{Bi}(a_2)/\mathrm{Bi}'(a_2) = 1/\sqrt{a_2}$. This ratio is small compared to 1 for $m \gtrsim 10^4$. The smallness of the right-hand side (RHS) of Eq. (16) means that X is close to the solution X_0 given by Eq. (6) and corresponding to Dirichlet's BC and $a_1 = -\zeta_q$. Searching $X = X_0 + X_{\mathrm{ev}}$, we can find from Eqs. (15) and (16) the evanescent correction X_{ev}. In the leading approximation in $1/m$ we have $X_{\mathrm{ev}} = -2n/m\sqrt{n^2-1}$ and $a_1 = -\zeta_q + (2/m)^{1/3} n/\sqrt{n^2-1}$. The main contribution to X_{ev} is thus of the order of the smallest contribution to X_0 [see Eq. (6)]. Deviation of a_1 from $-\zeta_q$ means that the radial function $\mathrm{Ai}(a_1 + u/u_m)$ is small but nonzero at the boundary. In air, the radial function $\mathrm{Bi}(a_2 + u/u_m)$ decreases very rapidly, as $\exp(-2\pi\sqrt{n^2-1}\,|u|/\lambda)$, with increasing $|u|$.

For the TM mode we have a similar situation. To get the dispersion equation for this case, it is sufficient to add n^2 in the denominator of the RHS of Eq. (16). Correspondingly, the values of X_{ev} and $a_1 + \zeta_q$ are smaller by a factor of $1/n^2$ compared to those in the TE case. Modifications of the first radial function $U_1(u/u_m)$ for the TE and TM modes when changing from the Dirichlet to air-dielectric BCs are illustrated by Fig. 3(b) for $m = 2 \times 10^4$ and $n = 2.2$.

Importantly, the dispersion equation (16) for the TE mode and its modification for the TM mode enable us to find X_{ev} with a higher accuracy, namely, up to the terms of the order of $m^{-5/3}$. Details of the derivation procedure can be found in Appendix B. Here we present the final result:

$$X_{\mathrm{ev}}^{\mathrm{TE}} = -\frac{2n}{\sqrt{n^2-1}}\frac{1}{m} - \frac{\zeta_q\, n(3-2n^2)}{6(n^2-1)^{3/2}}\left(\frac{2}{m}\right)^{5/3},$$
$$X_{\mathrm{ev}}^{\mathrm{TM}} = -\frac{2}{n\sqrt{n^2-1}}\frac{1}{m} - \frac{\zeta_q\,(3n^2-2)}{6n^3(n^2-1)^{3/2}}\left(\frac{2}{m}\right)^{5/3}. \tag{17}$$

It is necessary to keep in mind that the contribution Δ_1 to the Laplacian [see Eq. (7)] gives correction X_1 to the frequency parameter X. For Dirichlet's BCs, X_1 is given by Eq. (8). The question is whether weak modifications of the radial functions owing to the dielectric-air BCs influence X_1. It is clear that the weak and sharply decreasing evanescent parts of the radial functions give negligible corrections to X_1. It is clear also that corrections to the second contribution to X_1 in Eq. (8), which is already as small as $m^{-5/3}$, are negligible. However, correction $(\delta X_1)_{\mathrm{ev}}$ to the largest first contribution to X_1, which originates from the first term in Eq. (7), must be taken into account. This correction can be calculated in a

simple way with the help of relations of Appendix A: Instead of the integral $\int_0^\infty y^2 \mathrm{Ai}^2(y-\zeta_q)\,dy$ in Dirichlet's case, we have $\int_0^\infty y^2 \mathrm{Ai}^2(y-\zeta_q+\delta a_1)\,dy$, where $\delta a_1 \sim m^{-1/3} \ll 1$ is specified above for the TE and TM modes. In the linear approximation in δa_1, the ratio of the correction to the primary value is $-5\delta a_1/2\zeta_q$. Multiplying the first contribution to X_1 in Eq. (8) by this ratio, we get

$$(\delta X_1)_{\mathrm{ev}}^{\mathrm{TE}} = -\frac{\zeta_q n}{\sqrt{n^2-1}}\left(\frac{2}{m}\right)^{5/3},$$
$$(\delta X_1)_{\mathrm{ev}}^{\mathrm{TM}} = -\frac{\zeta_q}{n\sqrt{n^2-1}}\left(\frac{2}{m}\right)^{5/3}. \tag{18}$$

Collecting lastly all contributions to X, we have $(\omega Rn/cm)^2 = X_1 + X_2 + X_{\mathrm{ev}} + (\delta X_1)_{\mathrm{ev}}$. Here, the smallest contributions are of the order of $m^{-5/3}$. Extracting the square root from the right-hand side, using Eqs. (6), (8), (17), and (18), and keeping in $\sqrt{X}$ terms up to $\sim m^{-5/3}$ in the order of magnitude, we obtain finally for the frequency $\omega = \omega(q, p)$:

$$\frac{\omega Rn}{c} = m + \zeta_q\left(\frac{m}{2}\right)^{1/3} + (p+0.5)\sqrt{\eta} - \frac{P}{\sqrt{n^2-1}} + \frac{3\zeta_q^2}{20}\left(\frac{2}{m}\right)^{1/3} + \frac{\zeta_q(p+0.5)\eta^{3/2}}{6}\left(\frac{2}{m}\right)^{2/3} - \frac{\zeta_q P(3n^2-2P^2)}{6(n^2-1)^{3/2}}\left(\frac{2}{m}\right)^{2/3}, \tag{19}$$

where $P = n$ and $1/n$ for the TE and TM modes, respectively. The evanescent terms in this expression do not depend on the ratio $\eta = R/r$. In the case of sphere ($\eta = 1$), all terms of Eq. (19) coincide with the corresponding terms of [45,46]. To see this coincidence, it is sufficient to take into account that the orbital number ℓ (relevant to the spherical case) is linked to the azimuth and polar numbers by $\ell = m + p$, where $p \ll m$. Also, all terms of Eq. (19) coincide with the corresponding terms of [25–27]. These papers analyzed the scalar Helmholtz and eikonal equations for the spheroidal and toroidal geometries and postulated the presence of evanescent terms to get an agreement with the spherical case.

Within our vectorial perturbation theory, each of the last three terms in Eq. (19) comes from superposition of different contributions. Namely, it comes from high-order evanescent terms, from high-order scalar corrections relevant to the contribution Δ_1 in the Laplacian Δ, and from quadratic terms in the δ expansion of $\sqrt{1+\delta}$. The right structure of the final Eq. (19) provides strong evidence of the correctness of our theory.

Expansion (19) does not include terms of the order of $1/m$ and smaller. Definitely, this accuracy is sufficient for many practical purposes. Determination of smaller expansion terms for $\eta \neq 1$ seems to be highly problematic and greatly useless. First, smaller corrections are sensitive to fine shape features that cannot be described by the radii ratio η. In particular, such corrections are different for the spheroidal and toroidal geometries already within the scalar theory. Second, vectorial effects impose restrictions on the use of the scalar theories. In particular, vectorial coupling terms can give corrections $\delta\omega \sim \omega/m^2$. In essence, abandonment of the frequency corrections $\delta\omega \lesssim \omega/m^2$ makes our theory fairly simple and robust.

Consider now the possibility of modal anticrossings in the case of resonators made of isotropic optical materials. The necessary condition for an anticrossing is the equality $\omega_{\mathrm{TE}}(m, q_{\mathrm{e}}, p_{\mathrm{e}}) = \omega_{\mathrm{TM}}(m, q_{\mathrm{o}}, p_{\mathrm{o}})$, where the subscripts e and o refer to the radial and polar numbers of the TE and TM modes, respectively. It is easy to see that this condition cannot be fulfilled for $q_{\mathrm{e}} \neq q_{\mathrm{o}}$ and $m \gtrsim 10^3$. In the case $q_{\mathrm{e}} = q_{\mathrm{o}}$, the anticrossing condition gives, in the leading approximation, $\sqrt{\eta} = \sqrt{n^2-1}/n(p_{\mathrm{e}} - p_{\mathrm{o}})$. This condition can be fulfilled. According to Eq. (13), the operator $\hat{K}$ couples only the TE and TM modes with neighboring polar numbers. Thus, the case $p_{\mathrm{e}} - p_{\mathrm{o}} = 1$ is the most actual. With the index n ranging from 1.5 to 2.5, the required value of η varies from $\simeq$0.55 to 0.84. In reality, both the index n and the radii ratio η can be tuned continuously only slightly. This is why anticrossings of the TE and TM modes can occur only occasionally in the isotropic case. We will see in the next section that the situation changes dramatically in the anisotropic case.

IV. ANISOTROPIC VECTORIAL CASE

A. Modification of the basic relations

We assume now that the resonator is axially symmetric and anisotropic, so that its symmetry axis coincides with the z axis of a uniaxial crystal. In the Cartesian $x_1, x_2, x_3 = z$ coordinate system, the only nonzero components of the optical permittivity tensor $\hat{\varepsilon}$ are $\varepsilon_{11} = \varepsilon_{22} = n_{\mathrm{o}}^2$ and $\varepsilon_{33} = n_{\mathrm{e}}^2$, where n_{o} and n_{e} are the ordinary and extraordinary refractive indices. The ratio $\beta = (n_{\mathrm{o}}^2 - n_{\mathrm{e}}^2)/n_{\mathrm{o}}^2$ serves as the anisotropy parameter. It is very small for all known uniaxial crystals, $|\beta| \ll 1$. Generally, the optical permittivity tensor can be presented as $\hat{\varepsilon} = n_{\mathrm{o}}^2(\hat{1} - \beta\hat{\nu})$, where $\hat{1}$ is the unit tensor and the only nonzero component of $\hat{\nu}$ is $\nu_{33} = 1$. Components of $\hat{\nu}$ in our u, θ, φ coordinate system can be easily calculated; within the linear in θ approximation, the only nonzero components are $\nu_{\theta\theta} = 1$, $\nu_{\theta u} = \nu_{u\theta} = \theta$.

Maxwell's equations give straightforwardly without any approximations for the field components H_z and E_z representing the o and e modes, respectively:

$$\Delta H_z + k^2 n_{\mathrm{o}}^2 H_z = 0,\ \Delta E_z - \beta\frac{\partial^2 E_z}{\partial z^2} + k^2 n_{\mathrm{e}}^2 E_z = 0. \tag{20}$$

These equations show explicitly that there is no coupling between H_z and E_z in the bulk. While the equation for H_z already has the Helmholtz form, the equation for E_z acquires this form after a trivial rescaling: $z \to \tilde{z} = z/\sqrt{1-\beta} \simeq (1 + \beta/2)z$. Correspondingly, the radii ratio $\eta = R/r$ changes to $\eta_{\mathrm{e}} \simeq \eta(1+\beta/2)$ for the e modes. Since $|\beta| \ll 1$, the effects of the rescaling are small. As follows from the structure of Eqs. (20), the parameters $X_{o,e} = \omega^2 R^2 n_{\mathrm{o,e}}^2/m^2c^2$ have to be employed instead of $X = \omega^2 R^2 n^2/m^2c^2$ to analyze the effect of air-dielectric BCs on the WGM frequencies.

To modify the noncoupling terms in BCs (13), it is sufficient to change $n^2 \to n_{\mathrm{o}}^2$ in the last line. In the coupling terms (the second terms in the left- and right-hand sides), it is sufficient to employ n as the average index $(n_{\mathrm{o}} + n_{\mathrm{e}})/2$. This corresponds to the leading approximation in $1/m$ and β. The

point is that the anisotropic corrections to the coupling terms, see the above relations for $\hat{\varepsilon}$, are controlled by the product $\beta\theta$; they are small compared to the primary coupling terms. Note that the coupling terms in our BCs couple only o and e modes with neighboring polar numbers, i.e., obeying the selection rule $p_\mathrm{o} - p_\mathrm{e} = \pm 1$.

As follows from the above considerations, minor modifications in Eq. (19) are sufficient to get the frequencies $\omega_{\mathrm{o,e}}$: To change $n \to n_{\mathrm{o,e}}$, to change $\eta \to \eta_\mathrm{e}$ for the e modes, and to modify the definition of P, now $P = n_\mathrm{e}$ and $1/n_\mathrm{o}$ for the e and o modes. These modifications correspond greatly to an intuitive notion about the o and e modes. In many practical cases, high-order corrections in $1/m$ and β are not necessary, so that the expressions for $\omega_{\mathrm{o,e}}$ can be simplified. In particular, omission of the terms $\sim m^{-2/3}$ in a heuristically modified isotropic relation was sufficient for identification of the o,e modes in birefringent WGM resonators [18,32]. Employment of BCs (13) without modification of the non-coupling terms also makes sense: Within this approximation $\omega_{\mathrm{o,e}} = (cm/n_{\mathrm{o,e}}R)\,[1 + \cdots]$, where small correction terms in the square bracket depend only on n and $1/m$.

B. Anticrossings of o and e modes

In contrast to the isotropic case, crossings and anticrossings of WGMs are very likely in anisotropic crystals. The point is that (roughly) $\omega_{\mathrm{o,e}} \propto n_{\mathrm{o,e}}$. When tuning the resonator by means of temperature changes or application of a static electric field, the indices n_o and n_e change differently, so that the anticrossings become unavoidable and frequent [16,38,47]. To exemplify this issue, we indicate that the thermo-optic coefficients $n'_\mathrm{o} = dn_\mathrm{o}/dT$ and $n'_\mathrm{e} = dn_\mathrm{e}/dT$ in $LiNbO_3$ crystals differ roughly by 1 order of magnitude, leading to strongly different slopes of $\omega_\mathrm{o}(T)$ and $\omega_\mathrm{e}(T)$ for any combinations of modal numbers. A similar situation occurs for the field tuning employing the linear electro-optic effect [16].

Owing to the axial symmetry, anticrossings are forbidden for WGMs with different azimuth numbers, so that $m_\mathrm{e} = m_\mathrm{o} = m$ is a necessary anticrossing condition. This complies with the general symmetry requirements [35]. To analyze the anticrossing condition $\omega_\mathrm{o}(m, q_\mathrm{o}, p_\mathrm{o}) = \omega_\mathrm{e}(m, q_\mathrm{e}, p_\mathrm{e})$, we restrict ourselves to the first four terms of the frequency expansions. Then we have in the leading approximation in the anisotropy parameter β,

$$\zeta_{q_\mathrm{o}} - \zeta_{q_\mathrm{e}} = \beta\left(\frac{m}{2}\right)^{2/3} - \left[\frac{\sqrt{n^2-1}}{n} \pm \sqrt{\eta}\right]\left(\frac{2}{m}\right)^{1/3}, \quad (21)$$

where $\pm$ is the sign of $p_\mathrm{o} - p_\mathrm{e}$. For $|\beta|m \gg 1$, which is fulfilled practically for all uniaxial crystals, the second term in the right-hand side is relatively small. Thus, the relationship between the radial numbers q_o and q_e essentially depends on the product $\beta(m/2)^{2/3}$. Typically, its value is well above 1 and the sign can be different. Thus, the cases $q_\mathrm{o} \gg q_\mathrm{e}$ and $q_\mathrm{o} \ll q_\mathrm{e}$ are very likely.

Precise calculations of the absolute values of $\omega_{\mathrm{o,e}}$ on the basis of the anticrossing condition are of minor interest. Furthermore, they are not necessary to describe the anticrossing behavior, including the avoidance gap. This behavior is controlled by the coupling terms in the BCs. Below we analyze it within the linear approximation in β keeping only the first four terms in the expansion (19). This means that we use BCs (13) with $n = (n_\mathrm{o} + n_\mathrm{e})/2$.

As the first step of our analysis we set

$$\begin{aligned}
E_z &= c_1^\mathrm{e}\,\Theta_{p_e}\,\mathrm{Ai}\big(a_1^\mathrm{e} + u/u_m\big) \quad (u > 0)\\
H_z &= c_1^\mathrm{o}\,\Theta_{p_o}\,\mathrm{Ai}\big(a_1^\mathrm{o} + u/u_m\big) \quad (u > 0)\\
E_z &= c_2^\mathrm{e}\,\Theta_{p_e}\,\mathrm{Bi}\big(a_2^\mathrm{e} + u/u_m\big) \quad (u < 0)\\
H_z &= c_2^\mathrm{o}\,\Theta_{p_o}\,\mathrm{Bi}\big(a_2^\mathrm{o} + u/u_m\big) \quad (u < 0),
\end{aligned} \quad (22)$$

where $c_{1,2}^{\mathrm{o,e}}$ are arbitrary constants. The coefficients $a_{1,2}^{\mathrm{o,e}}$ obey Eqs. (15) with replacements $X \to X_{\mathrm{o,e}}$, $n \to n_{\mathrm{o,e}}$, and $p \to p_{\mathrm{o,e}}$. The difference between n_o and n_e is taken into account in the leading approximation. Substituting Eqs. (22) into BCs (13) we get the following set of four linear equations for c_1^e, c_2^e, c_1^o, and c_2^o:

$$\begin{aligned}
c_1^\mathrm{e}\Theta_\mathrm{e}\mathrm{Ai}\big(a_1^\mathrm{e}\big) + c_1^\mathrm{o}(\theta\Theta_\mathrm{o}/n)\mathrm{Ai}\big(a_1^\mathrm{o}\big) &= c_2^\mathrm{e}\Theta_\mathrm{e}\mathrm{Bi}\big(a_2^\mathrm{e}\big) + c_2^\mathrm{o} n\theta\Theta_\mathrm{o}\mathrm{Bi}\big(a_2^\mathrm{o}\big)\\
c_1^\mathrm{o}\mathrm{Ai}\big(a_1^\mathrm{o}\big) &= c_2^\mathrm{o}\mathrm{Bi}\big(a_2^\mathrm{o}\big)\\
c_1^\mathrm{e}\Theta_\mathrm{e}\mathrm{Ai}'\big(a_1^\mathrm{e}\big) + \frac{c_1^\mathrm{o}}{n}\left[\theta\Theta_\mathrm{o}\mathrm{Ai}'\big(a_1^\mathrm{o}\big) - \frac{\Theta'_\mathrm{o}u_m}{r\theta_m}\mathrm{Ai}\big(a_1^\mathrm{o}\big)\right] &= c_2^\mathrm{e}\Theta_\mathrm{e}\mathrm{Bi}'\big(a_2^\mathrm{e}\big) + c_2^\mathrm{o} n\left[\theta\Theta_\mathrm{o}\mathrm{Bi}'\big(a_2^\mathrm{o}\big) - \frac{\Theta'_\mathrm{o}u_m}{r\theta_m}\mathrm{Bi}\big(a_2^\mathrm{o}\big)\right]\\
c_1^\mathrm{e} n\left[\theta\Theta_\mathrm{e}\mathrm{Ai}'\big(a_1^\mathrm{e}\big) - \frac{\Theta'_\mathrm{e}u_m}{r\theta_m}\mathrm{Ai}\big(a_1^\mathrm{e}\big)\right] - c_1^\mathrm{o}\Theta_\mathrm{o}\mathrm{Ai}'\big(a_1^\mathrm{o}\big) &= c_2^\mathrm{e} n^3\left[\theta\Theta_\mathrm{e}\mathrm{Bi}'\big(a_2^\mathrm{e}\big) - \frac{\Theta'_\mathrm{e}u_m}{r\theta_m}\mathrm{Bi}\big(a_2^\mathrm{e}\big)\right] - c_2^\mathrm{o} n^2\Theta_\mathrm{o}\mathrm{Bi}'\big(a_2^\mathrm{o}\big).
\end{aligned} \quad (23)$$

The zero determinant condition for this set, $D = 0$, gives the necessary dispersion relation for ω. With the coupling terms omitted, it gives separate relations for ω_e and ω_o:

$$\frac{\mathrm{Ai}\big(\tilde{a}_1^\mathrm{e}\big)}{\mathrm{Ai}'\big(\tilde{a}_1^\mathrm{e}\big)} = \frac{\mathrm{Bi}\big(\tilde{a}_2^\mathrm{e}\big)}{\mathrm{Bi}'\big(\tilde{a}_2^\mathrm{e}\big)} \quad \text{and} \quad \frac{\mathrm{Ai}\big(\tilde{a}_1^\mathrm{o}\big)}{\mathrm{Ai}'\big(\tilde{a}_1^\mathrm{o}\big)} = \frac{1}{n^2}\frac{\mathrm{Bi}\big(\tilde{a}_2^\mathrm{o}\big)}{\mathrm{Bi}'\big(\tilde{a}_2^\mathrm{o}\big)}. \quad (24)$$

The tilde sign indicates that $a_{1,2}^{\mathrm{o,e}}$ are taken at zero coupling. Within our approximations, $\tilde{a}_1^{\mathrm{o,e}}$ are close to $-\zeta_{q_{\mathrm{o,e}}}$, $\tilde{a}_2^{\mathrm{o,e}} = a = (m/2)^{2/3}(n^2-1)/n^2 \gg 1$, and $\mathrm{Bi}(\tilde{a}_2^{\mathrm{o,e}})/\mathrm{Bi}'(\tilde{a}_2^{\mathrm{o,e}}) = 1/\sqrt{a} \ll 1$.

Set (23) can be strongly simplified. The main steps of our simplification procedure are as follows:

(1) We set $a_{1,2}^{\mathrm{o,e}} = \tilde{a}_{1,2}^{\mathrm{o,e}} - \tau_{1,2}^{\mathrm{o,e}}\delta_{\mathrm{o,e}}$, where $\delta_{\mathrm{o,e}} = \omega - \omega_{\mathrm{o,e}}$, $\tau_1^{\mathrm{o,e}} = n\tau$, $\tau_2^{\mathrm{o,e}} = \tau/n$, and $\tau = (2/m)^{1/3}R/c$.

(2) We employ the linear expansions of the Airy functions and their derivatives in $\delta_{\mathrm{o,e}}$. Using the Airy equation $y'' = xy$, we get rid of Ai'' and Bi''.

(3) We multiply the first and third of Eqs. (23) by Θ_e, the second and fourth equations by Θ_o, and integrate over $x = \theta/\theta_m$. Then the polar overlaps $J_1 = \langle\Theta_o(x)|x|\Theta_e(x)\rangle$ and $J_2 = \langle\Theta_e(x)|\Theta_o'(x)\rangle = -\langle\Theta_o(x)|\Theta_e'(x)\rangle$ appear; they are nonzero only for $|p_o - p_e| = 1$.

(4) Instead of deviations $\delta_{e,o}$ we introduce the normalized quantities $y_{o,e} = \sqrt{a}\tau\delta_{o,e}$, where $\sqrt{a}\tau = R\sqrt{n^2-1}/nc$. Also, we introduce two dimensionless coupling constants $g_1 = J_1\theta_m \ll 1$ and $g_2 = J_2 u_m/r\theta_m\sqrt{a} \ll 1$.

(5) We renormalize constants $c_{1,2}^{o,e}$: $c_{1,2}^{o,e}\mathrm{Ai}'(\tilde{a}_1^{o,e}) \to c_1^{o,e}$ and $c_2^{o,e}\mathrm{Bi}'(a) \to c_2^{o,e}$. This step is equivalent to multiplication of the determinant D by a constant. The dispersion equation $D = 0$ stays unchanged, but the Airy functions and their derivatives disappear.

After all, we arrive at the following expression for D:

$$D = \begin{vmatrix} 1 - ny_e & g_1/n^3 & 1 - y_e/n & -g_1 n \\ 0 & 1/n^2 - ny_o & 0 & -1 + y_o/n \\ 1 & g_1/n - g_2/n^3 & 1 - y_e/n & n(g_2 - g_1) \\ n(g_1 + g_2) & -1 & n^3(g_1 + g_2) & n^2 - ny_o \end{vmatrix}. \tag{25}$$

Generally, it is of fourth power in ω. With the coupling terms neglected ($g_{1,2} = 0$), the dispersion relation $D = 0$ gives the expected result: $y_o = 0$ and $y_e = 0$. Next, one can find analytically, or using MATHEMATICA, that within the quadratic approximation in y_e, y_o, and $g_{1,2}$,

$$D = n^4 y_o y_e - (g_1 + g_2)^2(n^2 - 1)^2/n^2. \tag{26}$$

Higher-order corrections to D are negligible for $|y_{o,e}|, |g_{1,2}| \ll 1$. Despite a rather complicated dependence of the elements of D on $g_{1,2}$, we have a simple final expression with the effective coupling strength $g_1 + g_2$.

The dispersion equation $D(\omega) = 0$ gives the generic solution for two frequencies,

$$\omega_\pm = [\omega_o + \omega_e \pm \sqrt{(\omega_o - \omega_e)^2 + 4\gamma^2}\,]/2, \tag{27}$$

where the only parameter specific for our case is

$$\gamma = (g_1 + g_2)(n^2 - 1)/n^3\sqrt{a}\tau. \tag{28}$$

Far from the anticrossing region, $|\omega_o - \omega_e| \gg |\gamma|$, we have almost undisturbed o and e modes with frequencies ω_e and ω_o. Within the narrow anticrossing region $|\omega_o - \omega_e| \lesssim \gamma$, a strong hybridization of the modes takes place. The minimum distance between the $\omega_\pm$ branches (the avoidance gap) is $2|\gamma|$. It takes place at $\omega_o = \omega_e$.

It is not difficult to express γ by the experimental parameters and modal numbers. We find first that

$$g_1 = \frac{J_1\eta^{3/4}}{m^{1/2}},\quad g_2 = \frac{J_2\eta^{1/4}n}{m^{1/2}\sqrt{n^2-1}},\quad \sqrt{a}\tau = \frac{\sqrt{n^2-1}}{n^2\,\Delta_\omega}, \tag{29}$$

where $\Delta_\omega = c/nR$ is the angular free spectral range. Both g_1 and g_2 are of the order of $m^{-1/2}$. The overlaps $J_{1,2}$ can be calculated using quantum-mechanical relations for the linear oscillator [35]:

$$\begin{aligned} x\Theta_p &= \sqrt{p/2}\;\Theta_{p-1} + \sqrt{(p+1)/2}\;\Theta_{p+1}, \\ d\Theta_p/dx &= \sqrt{p/2}\;\Theta_{p-1} - \sqrt{(p+1)/2}\;\Theta_{p+1}. \end{aligned} \tag{30}$$

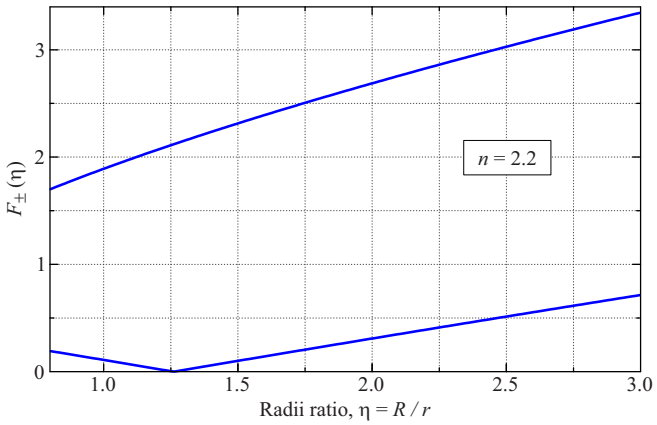

FIG. 4. Functions $F_\pm = \eta^{1/4}|1 \pm \eta^{1/2}\sqrt{1 - n^{-2}}|$ for $n = 2.2$.

Correspondingly, we have $J_1 = \sqrt{p_*/2}$ and $J_2 = \pm\sqrt{p_*/2}$, where $p_* = \max\{p_o, p_e\}$ and the sign $\pm$ corresponds to $p_o - p_e = \pm 1$. Using the above relations, we obtain a simple expression for the avoidance gap $2|\gamma|$:

$$\frac{2|\gamma|}{\Delta_\omega} = \eta^{1/4}\left(\frac{2p_*}{m}\right)^{1/2}|1 \pm \eta^{1/2}\sqrt{1 - n^{-2}}|\,. \tag{31}$$

Thus, the gap is not symmetric in the sign of $p_o - p_e$. The degree of asymmetry depends on η and n, as illustrated by Fig. 4.

Roughly, the gap is $\sim 10^{-2}\Delta_\omega$, in accordance with experiment. The smallness of γ/Δ_ω fully justifies the linear expansions of the Airy functions in $\delta_{o,e}$.

Our vectorial approach allows also for the description of polarization properties of the $\pm$ modes. Within the anticrossing region, $|\delta\omega| \lesssim 2\gamma$, a strong hybridization of the o and e modes occurs. This is indeed a generic feature of the anticrossing behavior. Far from the anticrossing points, $|\delta\omega| \gg 2\gamma$, the effect of vectorial coupling on the frequencies and polarizations of the ordinary and extraordinary WGMs is negligible.

C. Application to lithium niobate crystals

When dealing with experimental issues, it is useful to change from ω to the frequency $\nu = \omega/2\pi$. The natural frequency scale in the WGM experiments is the free spectral range $\Delta_\nu = \Delta_\omega/2\pi = c/2\pi nR$. It is only slightly different for the o and e modes.

A typical anticrossing experiment is as follows [16,47]: The WGM frequencies are slowly tuned by changing the temperature T or applying an electric field E_0. During this frequency tuning, the pump frequency ν_p is sweeping forth and back within a range of $\sim\Delta_\nu$. Typically, prism or fiber couplers are used to excite WGMs, and sharp drops of the transmitted pump power indicate crossing of very narrow WGM resonances. In this way, a two-dimensional ν-T (or ν-E_0) map of WGM resonances, including numerous anticrossings, can be obtained. For simplicity, we restrict ourselves to thermal tuning. The values of the avoidance gaps for the major o-e anticrossings as well as the frequency and temperature differences between them are of prime interest.

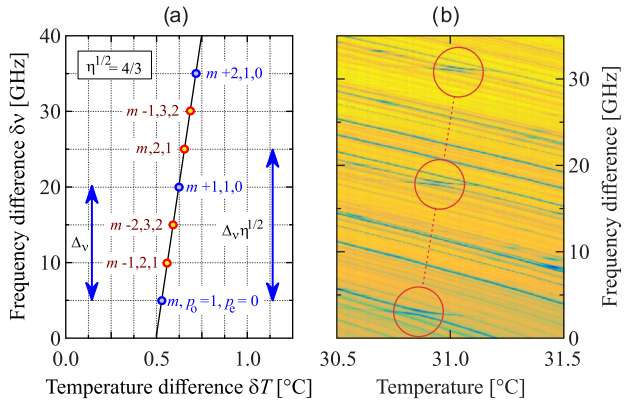

FIG. 5. (a) Neighboring anticrossings for $\sqrt{\eta} = 4/3$, fixed $q_{o,e}$, and different values of m and p_o with $p_o - p_e = 1$. Blue circles refer to $p_o = 1$, $p_e = 0$. The slope of the line comprising the anticrossings is ≃145 GHz/°C. (b) A fragment of the experimental ν-T frequency map obtained for a lithium niobate disk resonator with $R \simeq 1.35$ mm and $\eta \simeq 2$. The dashed red line is shown to guide the eye. Three neighboring anticrossings are highlighted. Different slopes ν'_o and ν'_e beyond the anticrossing regions are clearly seen.

In our experiments, we used axisymmetric anisotropic resonators with $R \simeq 1.35$ mm, $\eta = 1.5 - 2$, and $Q \sim 10^8$ made of MgO-doped (5 mol %) $LiNbO_3$ crystals. This uniaxial material possesses a large birefringence, $n_o \simeq 2.23$ and $n_e \simeq 2.15$, at $T \simeq 20\,^\circ$C and $\lambda \simeq 1\,\mu$m. Correspondingly, we have $m \simeq 2 \times 10^4$, $\beta \simeq 0.075$, $\beta(m/2)^{2/3} \simeq \zeta_{q_o} - \zeta_{q_e} \simeq 35$, and $\Delta_\nu \simeq 15$ GHz. For $q_e = 1$, we obtain $q_o \approx 50$. Excitation of o modes with so large radial numbers is not possible from outside.

Except for narrow anticrossing regions, the frequency map consists of two sets of almost straight parallel lines relevant to o and e modes [47]. The corresponding slopes are $\nu'_o = d\nu_o/dT \simeq -4.7$ and $\nu'_e = d\nu_e/dT \simeq -10.15$ GHz/K. These slopes incorporate not only the difference in n'_o and n'_e, but also the transverse thermal expansion of the resonator. The distances between the parallel lines in each set are controlled by the modal numbers in accordance with Eq. (19).

This structure of the frequency map allows us to make simple predictions for the anticrossing positions. They are illustrated by Fig. 5(a). Let an anticrossing with azimuth number m, radial numbers $q_{o,e}$, and polar numbers $p_{o,e}$ occur at certain frequency ν_0 and temperature T_0. What is then the anticrossing positions ν_1 and T_1 for the same $q_{o,e}$, $p_{o,e}$, and the azimuth number $m + 1$? Using the relations for $\omega(m, q, p)$ and $\nu'_{o,e}$, we get $\delta\nu = \nu_1 - \nu_0 \simeq \Delta_\nu$ and $\delta T = T_1 - T_0 \simeq \beta\Delta_\nu/2(\nu'_o - \nu'_e) \simeq 0.1\,^\circ$C. The avoidance gaps for these two anticrossings should be almost the same. Similarly, we obtain that $\delta\nu$ and δT increase by a factor of $\sqrt{\eta}$ for the change $p_{o,e} \to p_{o,e} + 1$ with the same m and $q_{o,e}$. The avoidance gap has to be larger here because of increasing $p_* = \max\{p_o, p_e\}$. Other changes of the modal numbers give much larger differences $\delta\nu$ and δT: For the change $q_o \to q_o - 1$ we obtain $\delta\nu \approx 20\Delta_\nu$ and $\delta T \approx 36\,^\circ$C. The interchange of p_o and p_e, reversing the sign of $p_o - p_e$, leads to $\delta\nu \simeq -2.6\sqrt{\eta}\Delta_\nu$ and $\delta T \simeq 6.7\sqrt{\eta}\,^\circ$C. Thus, the family of anticrossings relevant to Fig. 5(a) is expected to be the most accessible in experiment.

A fragment of the experimental frequency map shown in Fig. 5(b) comprises three major anticrossings separated by the frequency and temperature differences of ≃15 GHz and 0.08 C. The avoidance gaps for them are almost the same, about 400 MHz. No other major anticrossings were found within the frequency and temperature ranges used (≃37 GHz and 3 °C). Taking into account that $\eta \simeq 2$ for the actual resonator, we conclude about a good quantitative agreement between theory and experiment for the anticrossings with $p_e = 0$ and different values of m [blue circles in Fig. 5(a)]. The absence of anticrossings with higher polar numbers p_e is remarkable. Most probably, it is due to predominant excitation of the modes with $p_1 = 0$ with our prism coupler. An experimental study of anticrossings in cojunction with identification of all relevant mode numbers represents a much more difficult problem.

Above we restricted ourselves to the major anticrossings with the avoidance gaps of hundreds of megahertz. The total amount of anticrossings with the avoidance gaps exceeding the linewidth (within a kilohertz range) and accessible in our experiments is indeed much larger. The minor anticrossings are expected to be relevant to higher-order corrections in the vectorial perturbation theory.

V. SUMMARY

Within a simple perturbative approach to the scalar Helmholtz equation, employing the idea of strong localization of WGMs near the resonator rim, we have obtained explicit relations for the frequencies $\omega(m, q, p)$ accounting for the contributions $\delta\omega$ larger than ω/m^2. These contributions are shape-robust, being fully controlled by the major and minor curvature radii of the resonator R and r. They coincide with the contributions obtained earlier by solving the scalar Helmholtz and eikonal equations in the curvilinear spheroidal and toroidal coordinate systems [25–27].

Within the same perturbative approach, we have developed a full-scale vectorial WGM theory based on Maxwell's equations and true air-dielectric boundary conditions (BCs). This theory is also shape-robust and it possesses the same accuracy for the WGM frequencies. Furthermore, it is applicable not only to the resonators made of isotropic media, but also to optically anisotropic resonators possessing the axial symmetry. An essential element of our theory is employment the field component E_z and H_z as independent variables. Without any approximations, they obey two separate scalar Helmholtz equations, featuring no coupling in the bulk. The only source of coupling between E_z and H_z are BCs.

The BCs for E_z and H_z, as derived in a perturbative manner from true air-dielectric BCs, include both noncoupling and coupling terms. The noncoupling terms are responsible for the primary frequencies of two polarization types of WGMs, while the coupling terms determine the avoidance gaps during the anticrossings.

In the isotropic vectorial case, the noncoupling terms in the BCs for E_z and H_z provide not only the contributions to $\omega(m, q, p)$ known from scalar theories [25–27], but also evanescent contributions that are different for the quasi-TE and quasi-TM modes. For $R = r$, the contributions to ω_{TE} and ω_{TM} up to the terms $\propto m^{-5/3}$ coincide with the expansion

terms coming from the exact solution for the spherical geometry [45,46]. For $R \neq r$, our evanescent corrections coincide with those postulated in [25–27]. Thus, the expressions for WGM frequencies in the nonspherical case are derived from a true electromagnetic analysis. The coupling terms in the BCs are of minor importance in the isotropic case.

Our vectorial theory is applicable to the axisymmetric WGM resonators made of anisotropic materials, where the frequencies of ordinary (o) and extraordinary (e) modes are controlled by different refractive indices $n_{\rm o}$ and $n_{\rm e}$. The corresponding expressions for the frequencies $\omega_{\rm o}$ and $\omega_{\rm e}$ provide a solid basis for identification of WGMs in experiment. In contrast to the isotropic case, anticrossings of o and e modes are frequent, and the corresponding avoidance gaps are controlled by the coupling terms in the BCs for E_z and H_z. The expressions for the avoidance gaps, as derived within our theory, provide important predictions for experiment. These predictions are confirmed in experiments with axially symmetric WGM resonators made of $LiNbO_3$ crystals.

APPENDIX A: INTEGRALS WITH AIRY FUNCTIONS

Let ζ_q be the qth zeroth of $\mathrm{Ai}(-y)$. Then, the function $f_q(y) = \mathrm{Ai}(y - \zeta_q)$ with $q = 1, 2, \ldots$ is zero at $y = 0$, obeys the Airy equation $f_q'' = (y - \zeta_q) f_q$, and tends rapidly to zero for $y \to \infty$. Consider the sequence of simple identities employing partial integration:

$$\begin{aligned}(\zeta_{q_1} - \zeta_{q_2}) &\int_0^\infty f_{q_1} f_{q_2} dy \\ &= \int_0^\infty (\zeta_{q_1} - y + y - \zeta_{q_2}) f_{q_1} f_{q_2} dy \\ &= \int_0^\infty (f_{q_2}'' f_{q_1} - f_{q_1}'' f_{q_2}) dy \\ &= f_{q_2}'(0) f_{q_1}(0) - f_{q_1}'(0) f_{q_2}(0) = 0. \end{aligned} \tag{A1}$$

It proves that $\int_0^\infty f_{q_1}(y) f_{q_2}(y) dy = 0$ for $q_1 \neq q_2$. The same proof and the same orthogonality relation are valid for the set of functions $\tilde{f}_q = \mathrm{Ai}(y - \zeta_q')$, with ζ_q' being the qth zero of $\mathrm{Ai}'(-y)$.

Consider the function $f = \mathrm{Ai}(y - \zeta)$ with an arbitrary parameter ζ. It obeys the equation $f'' = (y - \zeta) f$. Analogously to Eqs. (A1) we obtain

$$(\zeta - \zeta_q) \int_0^\infty f f_q \, dy \equiv -\mathrm{Ai}(-\zeta)\mathrm{Ai}'(-\zeta_q). \tag{A2}$$

The RHS is zero for $\zeta = \zeta_q$. Its linear expansion in $\zeta - \zeta_q$ leads to the equality $\int_0^\infty f_q^2 \, dy = [\mathrm{Ai}'(-\zeta_q)]^2$. Repeating the same procedure with ζ_q' and $\tilde{f}_q$, we obtain that $\int_0^\infty \tilde{f}_q^2 \, dy = \zeta_q' \mathrm{Ai}^2(-\zeta_q')$. Thus, the normalization constant $C_q = 1/|\mathrm{Ai}'(-\zeta_q)|$ and $1/|\mathrm{Ai}(-\zeta_q')|\sqrt{\zeta_q'}$ for Dirichlet's and Neumann's BCs, respectively.

In a similar manner one finds the following for the overlap integral of the functions $f_{q_1}(y)$ and $\tilde{f}_{q_2}(y)$ with arbitrary radial numbers q_1 and q_2:

$$(\zeta_{q_1} - \zeta_{q_2}') \int_0^\infty f_{q_1} \tilde{f}_{q_2} \, dy \equiv \mathrm{Ai}'(-\zeta_{q_1})\mathrm{Ai}(-\zeta_{q_2}'). \tag{A3}$$

The starting point of the subsequent considerations is the lowering relation of Aspens [44],

$$\begin{aligned}\int_0^\infty x^n \mathrm{Ai}^2(x - y) dx &= \frac{n}{2n+1}\left(\frac{d^2}{2dy^2} + 2y\right) \\ &\times \int_0^\infty x^{n-1} \mathrm{Ai}^2(x - y) dx, \end{aligned} \tag{A4}$$

which is valid for $n > 0$ and any real y. For $n = 1$ it gives

$$\begin{aligned}\int_0^\infty x \mathrm{Ai}^2(x - y) dx &\equiv \frac{\mathrm{Ai}(-y)\mathrm{Ai}'(-y)}{3} \\ &+ \frac{2y}{3} \int_0^\infty \mathrm{Ai}^2(x - y) dx. \end{aligned} \tag{A5}$$

At $y = \zeta_q$ and ζ_q', the first contribution is zero and the second one is calculated above. Anyhow, we have $\int_0^\infty y f_q^2 dy / \int_0^\infty f_q^2 dy = 2\zeta_q/3$ and the same integral relation between $\tilde{f}_q$ and ζ_q'. With $n = 2$, the first (differential) contribution in the right-hand side of Eq. (A4) is zero again, and the second contribution can be calculated using Eq. (A5). Thus, we obtain $\int_0^\infty y^2 f_q^2 dy / \int_0^\infty f_q^2 dy = 8\zeta_q^2/15$ and the same integral relation between $\tilde{f}_q$ and ζ_q'.

APPENDIX B: PERTURBATIVE SOLUTION FOR $X_{\rm ev}$

We search for the solution of Eq. (16), relevant to the TE mode, in the form $X = X_0 + X_{\rm ev}^{\rm TE}$, where X_0 is given by Eq. (6) and $a_1(X_0) = -\zeta_q$. Then we have $a_1 = -\zeta_q - s$, where $s = (m/2)^{2/3} X_{ev}^{\rm TE}$. Expanding $\mathrm{Ai}(-\zeta_q - s)$ and $\mathrm{Ai}'(-\zeta_q - s)$ up to cubic and quadratic in s terms, respectively, and using the Airy equation, we obtain for the LHS of Eq. (16): LHS $\simeq -s - \zeta_q s^3/3$. In the RHS, it is sufficient to employ the asymptotic relation $\mathrm{Bi}(a_2)/\mathrm{Bi}'(a_2) = 1/\sqrt{a_2}$. Using Eq. (15) for $a_2(X)$, we expand the RHS in $\varepsilon = (2/m)^{1/3}$ and s, leading to

$$\mathrm{RHS} \simeq \frac{n\,\varepsilon}{\sqrt{n^2-1}} + \frac{\zeta_q\, n\, \varepsilon^3}{2(n^2-1)^{3/2}} + \frac{s\, \varepsilon^3}{2(n^2-1)^{3/2}}. \tag{B1}$$

To solve equation $\mathrm{LHS}(s) = \mathrm{RHS}(\varepsilon, s)$, we search $s = c_1\varepsilon + c_2\varepsilon^2 + c_3\varepsilon^3$. The higher-order terms would give an excessive accuracy for $X_{\rm ev}^{\rm TE}$. Furthermore, one can find that the last term in Eq. (B1) is also negligible, so that we can set $c_2 = 0$. After that we obtain easily that $X_{\rm ev}^{\rm TE}$ is given by Eq. (17). Repeating the same calculation procedure for the TM mode we obtain Eq. (17) for $X_{\rm ev}^{\rm TM}$. One can make sure that the neglected terms lead to higher-order (in ε) corrections to $X_{\rm ev}$.

[1] K. J. Vahala, Nature (London) **424**, 839 (2003).

[2] L. Maleki, V. S. Ilchenko, A. A. Savchenkov, and A. B. Matsko, in *Practical Applications of Microresonators in Optics and Photonics*, edited by A. B. Matsko (CRC Press, Boca Raton, FL, 2009).

[3] A. B. Matsko and V. S. Ilchenko, IEEE J. Quantum Electron. **12**, 3 (2006).

[4] V. S. Ilchenko and A. B. Matsko, IEEE J. Quantum Electron. **12**, 15 (2006).

[5] V. S. Ilchenko, A. A. Savchenkov, A. B. Matsko, and L. Maleki, Phys. Rev. Lett. **92**, 043903 (2004).

[6] J. U. Fürst, D. V. Strekalov, D. Elser, A. Aiello, U. L. Andersen, Ch. Marquardt, and G. Leuchs, Phys. Rev. Lett. **105**, 263904 (2010).

[7] T. Beckmann, H. Linnenbank, H. Steigerwald, B. Sturman, D. Haertle, K. Buse, and I. Breunig, Phys. Rev. Lett. **106**, 143903 (2011).

[8] P. Del'Haye, A. Schliesser, O. Arcizet, T. Wilken, R. Holzwarth, and T. J. Kippenberg, Nature **450**, 1214 (2007).

[9] T. J. Kippenberg, R. Holzwarth, and S. A. Diddams, Science **332**, 555 (2011).

[10] F. Vollmer and A. Arnold, Nat. Methods **5**, 591 (2008).

[11] T. Herr, V. Brasch, J. D. Jost, C. Y. Wang, N. M. Kondratiev, M. L. Gorodetsky, and T. J. Kippenberg, Nat. Photon. **8**, 145 (2014).

[12] I. S. Grudinin, A. B. Matsko, A. A. Savchenkov, D. Strekalov, V. S. Ilchenko, and L. Maleki, Opt. Commun. **265**, 33 (2006).

[13] D. K. Armani, T. J. Kippenberg, S. M. Spillane, and K. J. Vahala, Nature (London) **421**, 925 (2003).

[14] H. Lee, T. Chen, J. Li, K. Y. Yang, S. Jeon, O. Painter, and K. J. Vahala, Nat. Photon. **6**, 369 (2012).

[15] Y. Louyer, D. Meschede, and A. Rauschenbeutel, Phys. Rev. A **72**, 031801(R) (2005).

[16] D. V. Strekalov, Ch. Marquardt, A. B. Matsko, H. G. L. Schwefel, and G. Leuchs, J. Opt. **18**, 123002 (2016).

[17] M. Mohageg, A. Savchenkov, and L. Maleki, Opt. Express **15**, 4869 (2007).

[18] J. Fürst, B. Sturman, K. Buse, and I. Breunig, Opt. Express **24**, 20143 (2016).

[19] P. M. Morse and H. Feshbach, *Methods of Theoretical Physics* (McGraw-Hill, New York, 1953).

[20] M. L. Gorodetsky, *High-Q Optical Microresonators* (Fizmatgiz, Moscow, 2011), in Russian.

[21] A. N. Oraevsky, Quantum Electron. **32**, 377 (2002).

[22] B. Makkinejad and G. W. Ford, Phys. Rev. B **44**, 8536 (1991).

[23] Yu. V. Prokopenko, T. A. Smirnova, and Yu. F. Filippov, Sov. Tech. Phys. **49**, 459 (2004).

[24] M. Ornigotti and A. Aiello, Phys. Rev. A **84**, 013828 (2011).

[25] M. Gorodetsky and A. Fomin, IEEE J. Sel. Top. Quantum Electron. **12**, 33 (2006).

[26] M. L. Gorodetsky and Y. A. Demchenko, Proc. SPIE **8236**, 823623 (2012).

[27] Yu. A. Demchenko and M. L. Gorodetsky, J. Opt. Soc. Am. B **30**, 3056 (2013).

[28] I. Breunig, B. Sturman, F. Sedlmeir, H. G. L. Schwefel, and K. Buse, Opt. Express **21**, 30683 (2013).

[29] V. M. Babic and V. S. Buldyrev, *Short-Wavelength Diffraction Theory: Asymptotic Methods*, (Springer, New York, 1991).

[30] J. B. Keller and S. I. Rubinow, Ann. Phys. **9**, 24 (1960).

[31] J. Li, H. Lee, K. Yang, and K. Vahala, Opt. Express **20**, 26337 (2012).

[32] G. Schunk, J. U. Fürst, M. Förtsch, D. V. Strekalov, U. Vogl, F. Sedlmeir, H. G. L. Schwefel, G. Leuchs, and Ch. Marquardt, Opt. Express **22**, 30795 (2014).

[33] M. Oxborrow, IEEE Trans. Microwave Theory Tech. **55**, 1209 (2007).

[34] X. Du, S. Vincent, and T. Lu, Opt. Express **21**, 22012 (2013).

[35] L. D. Landau and E. M. Lifshitz, *Quantum Mechanics* (Pergamon Press, New York, 1977), p. 302.

[36] L. Novotny, Am. J. Phys. **78**, 1199 (2010).

[37] T. Carmon, H. G. L. Schwefel, L. Yang, M. Oxborrow, A. D. Stone, and K. J. Vahala, Phys. Rev. Lett. **100**, 103905 (2008).

[38] W. Weng and A. Luiten, Opt. Lett. **40**, 5431 (2015).

[39] J. Zhu, S. K. Ozdemir, Y.-F. Xiao, L. Li, L. He, D.-R. Chen, and L. Yang, Nat. Photon. **4**, 46 (2009).

[40] Y. Hara, T. Mukaiyama, K. Takeda, and M. Kuwata-Gonokami, Phys. Rev. Lett. **94**, 203905 (2005).

[41] L. I. Deych and O. Roslyak, Phys. Rev. E **73**, 036606 (2006).

[42] G. B. Arfken and H. G. Weber, *Mathematical Methods for Physicists* (Academic Press, New York, 2001).

[43] M. Abramowitz and I. A. Stegun, *Handbook of Mathematical Functions* (Dover Publications, New York, 1972), p. 367.

[44] O. Vallee and M. Soares, *Airy Functions and Applications to Physics* (World Scientific, Singapore, 2004), p. 56.

[45] C. C. Lam, P. T. Leung, and K. Young, J. Opt. Soc. Am. B **9**, 1585 (1992).

[46] S. Schiller, Appl. Opt. **32**, 2181 (1993).

[47] Ch. S. Werner, B. Sturman, E. Podivilov, S. Kini Manjeshwar, K. Buse, and I. Breunig, Opt. Express **26**, 762 (2018).